JOURNAL OF SOLID STATE CHEMISTRY **123,** 1–13 (1996)
ARTICLE NO. 0145

A General Survey of Quartz and Quartz-like Materials: Packing Distortions, Temperature, and Pressure Effects

E. Philippot, D. Palmier, M. Pintard, and A. Goiffon

Laboratoire de Physicochimie des Matériaux Solides, UM II, URA D0407-CNRS, cc003, Place E. Bataillon, F-34095 Montpellier Cedex 5, France

Received July 26, 1995; in revised form November 13, 1995; accepted November 16, 1995

A general survey of quartz and quartz-like structures (SiO_2, GeO_2, and MXO_4 with M = Al, Ga, Fe and X = P, As) has been undertaken to ascertain the effects of pressure and temperature on the quartz framework. All the quartz isotype crystal structures and their variations with respect to pressure and temperature can be expressed in terms of M–X (the nonbonded radius sum) and M–O–X (the corresponding angle). Thus, crystal packing can be described by the geometrical characteristics of MX_4 (or XM_4) tetrahedral units, such as M–X–M angle distortions, M–X lengths, and c/a ratios. MO_4 and XO_4 tetrahedral distortions can be closely related to the M–O–X angle. Crystal structure distortions expressed by the M–O—X angle lead to different physical properties. Density, piezoelectric coupling coefficient of AT cut, and dielectric constant anisotropy are linearly related to the M–O–X value. Thus, the knowledge of the M–O–X value allows prediction of the physical properties of quartz-like crystals that have not been synthesized. In conclusion, all the crystal structures and the physical properties of the quartz-like materials can be expressed in terms of only the M–O–X angle.

I. INTRODUCTION

Research has been carried out over the past few years on MXO_4 quartz-like materials (M = B, Al, Ga, Fe, Mn and X = P, As). For some of these compositions (M = Al, Ga and X = P, As), refined crystal structures (1) have been accurately determined, and investigations have been initiated to gauge their crystal growth conditions (2–4) and piezoelectric properties (2, 4–7). During the course of this research, some similarities and some drastic differences among the members of this series have become apparent. For example, the continuous solid solution $Al_{(1-x)}Ga_xPO_4$ for $0 \leq x \leq 1$ (8), for which the cell volume is constant ($V \approx 230 \pm 1$ Å^3), suggests that a very similar structural packing scheme characterizes the end member compounds $AlPO_4$ (berlinite) and $GaPO_4$. From this analogy, it was possible to synthesize, by hydrothermal crystal growth, large as-grown crystals of $GaPO_4$ from berlinite seeds (9). Nevertheless, while berlinite exhibits an α–β transition as in quartz, this inversion is absent in $GaPO_4$. These different behaviors have already been investigated in some depth, in particular the mechanism of the α–β transition and SiO_2 polymorphism (10, 11). Studies of quartz analogs have been less exhaustive (12–14).

Although $AlPO_4$ and SiO_2 polymorphic varieties are closely related, those of the other compounds are more limited. In a previous paper, devoted to the existence of the α–β transition in MXO_4 quartz-like materials (15), we demonstrated the prime importance of the role of nonbonded M–X interactions (16–18). The M–X distance, defined as the nonbonded radius sum, controls the structure packing. According to this analysis, as M–O and X–O distances increase, based on the ionic radii from Shannon and Prewitt (19), the distortion of the tetrahedral chain will increase with an M–O–X angle (θ) decrease and a concomitant increase of the tilt angle, δ (20). This increased distortion requires more energy to allow the α–β transition, and the transition will not occur when $\delta \geq 22°$ or $\theta \leq 136°$ (15).

On this basis, we want to extend this general survey of crystal structures of quartz and quartz-like materials, in particular to account for the role of temperature and pressure, on the nonbonded M–X distance and the correlated M–O–X angle, θ (or tilt angle δ). As a result, close relations may be revealed between the crystal structure distortions described by the M–O–X angle and different physical properties, such as densities, piezoelectric coupling coefficients, elastic constants, and anisotropies in the dielectric constants.

II. COMPARISON AND DISTORTION OF MXO_4 STRUCTURE PACKING

Characteristic data of all known (or assumed) quartz-like material structures are summarized in Table 1. The most interesting results of our previous work (15) on the relation between structural distortions and the existence of the α–β transition in quartz and quartz-like materials are schematized in Fig. 1. When the crystal structure deviates

0022-4596/96 $18.00

TABLE 1
Characteristic Crystal Structure Parameters of All Known (or Assumed) Quartz-Like Materials

								[θ]		[M–X]	
	Tetra.	c/a	V (Å^3)	bond (Å)	[bond] (Å)	δ (°)	[δ] (°)	theo. (°)	exp. (°)	theo. (Å)	exp. (Å)
	BO_4			*1.46*							
BPO_4		2.22	172		*1.49*		≈25	≈132		2.72	
	PO_4			*1.52*							
	BO_4			*1.46*							
$BAsO_4$		2.26	186		*1.58*		≈30	≈125		2.80	
	AsO_4			*1.70*							
	SiO_4	1.10	113								
SiO_2				1.608	1.608	16.3	16.3	144.8	143.7	3.06	3.057
	2×	2.20	226								
	AlO_4			1.736		16.2					
$AlPO_4$		2.22	231		1.628		17.6	142.8	142.4	3.08	3.085
	PO_4			1.521		18.9					
	GaO_4			1.815		20.8					
$GaPO_4$		2.25	229		1.670		23.3	135.4	134.6	3.09	3.085
	PO_4			1.525		25.7					
	GeO_4	1.13	122								
GeO_2				1.739	1.739	25.7	25.7	131.7	130.1	3.16	3.153
	2×	2.26	244								
	FeO_4			1.854		19.3					
$FePO_4$		2.23	247		1.691		21.5	137.7	137.8	3.14	3.161
	PO_4			1.527		23.7					
	AlO_4			1.742		21.8					
$AlAsO_4$		2.23	245		1.704		22.6	137.0	135.4	3.16	3.153
	AsO_4			1.665		23.4					
	GaO_4			1.771		25.6					
$GaAsO_4$		2.28	245		1.746		26.2	131.1	129.9	3.17	3.163
	AsO_4			1.721		26.8					
	FeO_4			*1.85*							
$FeAsO_4$		2.23	263		*1.775*		≈26	≈130		3.22	
	AsO_4			*1.70*							

Note. Italics mean data from nonrefined crystal structures.

markedly from the ideal β-quartz configuration ($\delta \geq 22°$ or M–O–$X(\theta) \leq 136°$), other phase transitions (for example, α-quartz → cristobalite at 1206 K for $GaPO_4$) or chemical decomposition are observed instead.

These angles, δ and θ, reflect the intertetrahedral distortions in the helical chains, as also indicated by the c/a ratio. The ideal value of the c/a ratio for the quartz structure is $c/a = (3/2)\sqrt{3} - 1 = 1.0981$ (or 2×1.0981 for quartz-like materials) at room temperature (21). The more that actual ratios exceed this value, the more the distortions are important. For the known quartz-like structures, this ratio ranges from 2.20 (SiO_2) to 2.28 ($GaAsO_4$) (Table 1). Similarly, these crystal structure distortions may be expressed in terms of the M–O–X angle, because the c/a ratio varies linearly with this angle (Fig. 2). Thus, the c/a ratio can be used to express the overall distortion of these structures.

On the other hand, the local distortion (or intratetrahedral distortion) can be estimated by the relation

$$\Delta x = d_1 \cos\frac{\alpha_1}{2} - d_2 \cos\frac{\alpha_2}{2}, \qquad [1]$$

where d_1 and d_2 are the A–$O_{(1)}$ and A–$O_{(2)}$ distances with $A = M, X$ and α_1 and α_2 their corresponding angles $O_{(1)}$–A–$O_{(1)}$ and $O_{(2)}$–A–$O_{(2)}$ (1). The same linear relation exists for the total value, $\sum \Delta x$, of the individual tetrahedra as a function of the M–O–X angle (θ) (Fig. 3). Thus, the

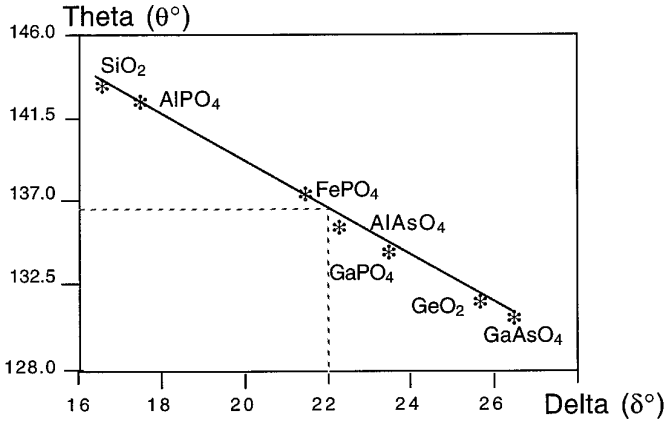

FIG. 1. Evolution of the bridging angle M–O–X, θ, in terms of the mean value of the tilt angle, δ*, of MO_4 and XO_4 tetrahedra. The theoretical evolution from (15) is plotted in full line. The α–β transition disappears for structures that have a θ value $\leq 136°$ or a δ value $\geq 22°$ at ambient conditions. *δ is the tilt angle between β- and α-quartz crystal structures.

M–O–X value describes intra- as well as intertetrahedral structure distortions.

The importance of this M–O–X angle has led us to consider the ''one angle'' or ''nonbonded'' radii defined by O'Keeffe and co-workers (17, 18). Experimental cell parameters and values calculated from theoretical M–X distances are presented in Table 1. Theoretical values of M–X distances (Table 2) have been obtained from (17, 18). Ga and Al show similar nonbonded radii, and thus give similar M–X distances; P–Ga and P–Al are 3.09 and 3.08 Å, respectively. The experimental and theoretical values for the tilt angle, δ, are in good agreement. The tilt can also be related to the M–O–X angle, θ, through the relation from (20),

$$\cos\theta = \frac{3}{4} - \left[\cos\delta + \frac{1}{2\sqrt{3}}\right]^2. \qquad [2]$$

Hill and Gibbs (22) have proposed a linear relationship

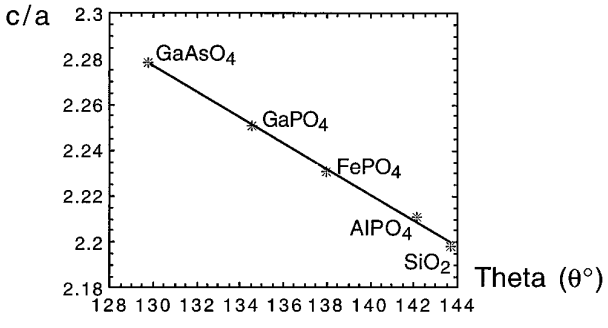

FIG. 2. Evolution of the c/a ratio in terms of the bridging angle M–O–X, θ.

TABLE 2
Nonbonded Radii of Tetrahedral Elements from Refs. (17, 18)

Atom	Nonbonded radius (Å)
B	1.26
O	1.12
Al	1.62
Si	1.53
P	1.46
Ga	1.63
As	1.54
Fe^{III}	1.68
Ge	1.58

between log sin[(Si–O–Si)/2] and log d(Si–Si). Although this correlation is approximately confirmed for silicates and for SiO_2 and GeO_2 with an increase on pressure, it is not predictive for quartz-like materials. Thus, M–X interactions cannot completely describe crystal structure distortions.

In brief, M and X cations determine the cell volumes of these materials (Table 1) through their mutual repulsion (nonbonded radii), whereas the anion–cation interactions influence intra- and intertetrahedral distortions (bridging angle θ or tilt angle δ) through the bond lengths (M–O and X–O), as reflected by the atomic size (ionic or covalent radii). As the nonbonded M–X distances are of prime importance on describing the packing schemes of these crystal structures, we have undertaken an analysis of quartz and quartz-like structures only in terms of MX_4 (or XM_4) tetrahedra and M–O–X bridging angles (Fig. 4).

In Fig. 5 the angular characteristics of the tetrahedra are summarized for all known quartz analogs in terms of

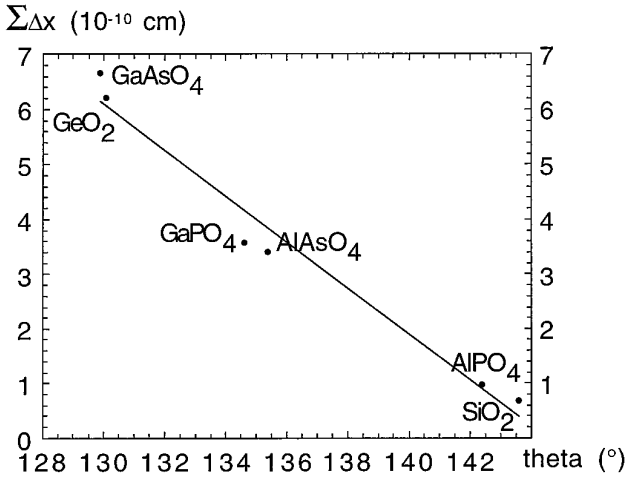

FIG. 3. Evolution of the intratetrahedral distortions in terms of the bridging angle M–O–X, θ. ($\Sigma\Delta x = \Delta xMO_4 + \Delta xXO_4$)

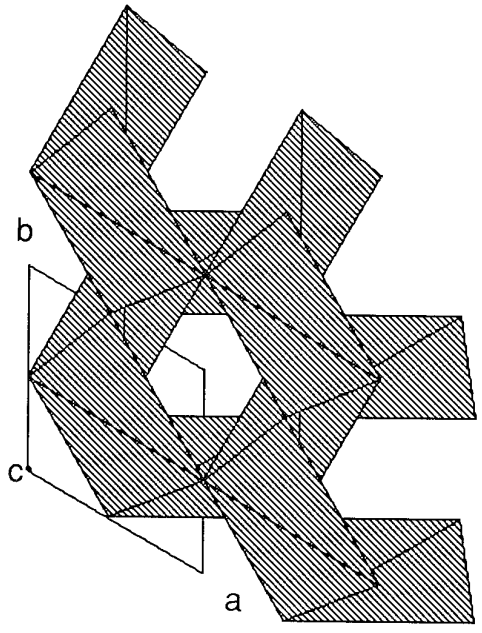

FIG. 4. Projection parallel to the *c* axis of the MXO_4 crystal structure using MX_4 (or XM_4) tetrahedra.

the *M*–O–*X* angle. The smallest *M*–O–*X* angle (≈90°) corresponds to *X* and *M* atoms belonging to a single tetrahedral chain parallel to the *c* axis. All other angles represent *M* and *X* atoms that bridge the intertwined chains (Fig. 6). It can be observed that, at room temperature and pressure, these tetrahedra are flattened along the Z direction (≈90 and ≈105° for *X*–*M*–*X* (*M*–*X*–*M*) angles perpendicular and parallel to the Z direction). All *X*–*M*–*X* angles vary linearly with *M*–O–*X*, and the more the angles are large, the more the variations are important; Δ(*M*–*X*–*M*) is close to 1.0°, 2.0°, 4.6°, and 5.9° for the end member compounds SiO_2 and $GaAsO_4$ when the

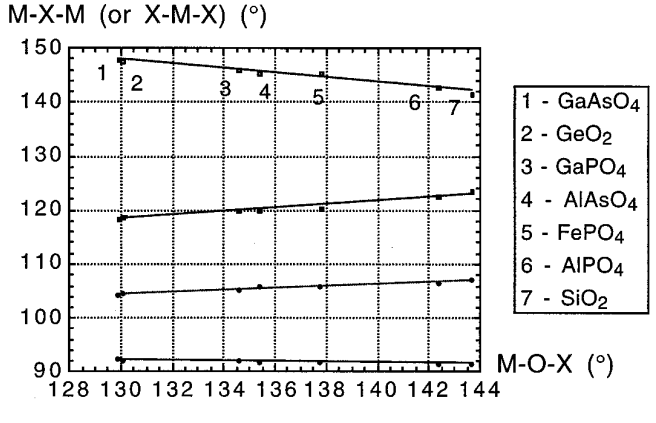

FIG. 5. Evolution of tetrahedral angles in MX_4 (or XM_4), in terms of the *M*–O–*X* angle.

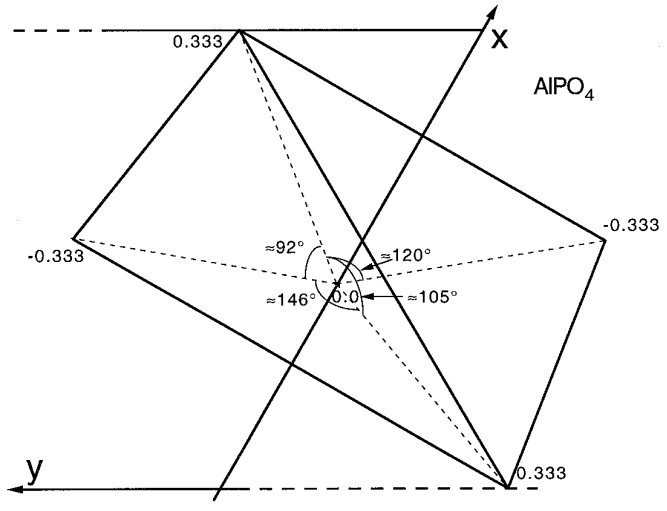

FIG. 6. Example of MX_4 tetrahedron: AlP_4 in $AlPO_4$.

M–*X*–*M* angle increases from 90°, 105°, 120°, and 145°, respectively (Fig. 5).

III. GENERAL SURVEY OF TEMPERATURE AND PRESSURE EFFECTS ON CRYSTAL STRUCTURE DEFORMATIONS OF QUARTZ AND QUARTZ-LIKE MATERIALS

The behavior of quartz-like materials is delimited by reconstructive changes that occur at high temperatures and pressures. Nevertheless, the stability range of the α-quartz structure is fairly extensive as a function of pressure. In general, the stability range is bounded in temperature by structural transition, melting, or chemical decomposition (12–14, 23, 24) and under pressure by transition (coordination change) (25, 26) or amorphization (27–31).

(*a*) *Temperature Effect*

The effect of temperature on these materials has not been as thoroughly investigated as those induced by pressure, with the exception of quartz itself. Nevertheless, some of these solids have been investigated (1, 32–37), and all the results lead to the same conclusion: all of the *M*–*X*–*M* (or *X*–*M*–*X*) angle evolve with temperature on the same way. In Fig. 7, we report data for α-quartz from (33, 35) and (32) at low and high temperature, respectively. The variations are limited by the α–β structure transition at 846 K. In this range, we observe that the intrachain angle remains constant while the interchain angles are more sensitive to temperature since they are larger.

(*b*) *Pressure Effect*

The pressure effect has been much more intensively investigated (38–44) than the temperature effect. The crys-

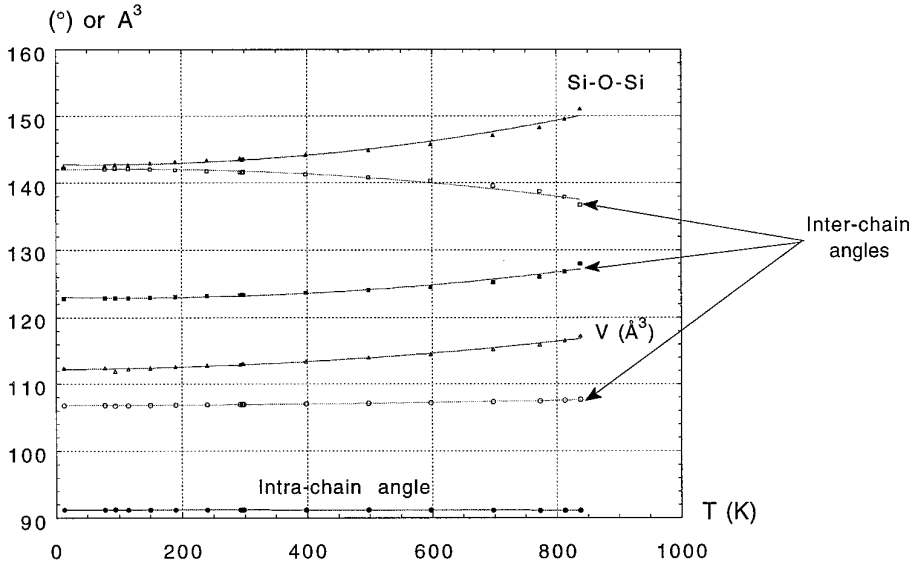

FIG. 7. Evolution of the four independent tetrahedral angles, X–M–X, of quartz in the temperature range 13–838 K. In the same range, evolution of the cell volume and the Si–O–Si angle. (All data have been fitted with a second order polynomial law.)

tal structure deformations are very sensitive to pressure. For all compounds, the same behavior is observed, and so we present only one example (Figs. 8 and 9), berlinite, $AlPO_4$ (41).

In projection, the longest tetrahedral edge, opposite to the largest angle (≈145° at standard pressure), does not change with higher pressure, whereas, the edge corresponding to the angle close to 120° is shortened. Consequently, the first angle must increase while the other must decrease, as confirmed by the evolution of the tetrahedral angles M–X–M in Fig. 9.

From this figure, one can ascertain the great stability of the intrachain angle (91.4° to 92.0°) over the entire pressure range investigated. This angle is characteristic of the helical chain along the c axis. All of the crystal structures that have been investigated in terms of pressure exhibit the same behavior, as also revealed by the $\Delta a/a$ and $\Delta c/c$ sensitivity (Fig. 10). In general, the compressibility of these structures exhibits the same anisotropy, with $\Delta c/c \approx 2(\Delta a/a)$. Variation in $\Delta c/c$ is due to the compressibility of the helical chains. Since the M–X–M angle remains constant, this compressibility reflects the M–X nonbonded distance. Conversely, the a axis shortening can be attributed to the compressibility of the helical chain packing related to the most pressure sensitive angles, X–M–X, between helical chains (Fig. 8 and 9). In brief, for all the quartz materials, the compressibility along the helical chain is less pronounced than the compressibility associated with the packing of chains.

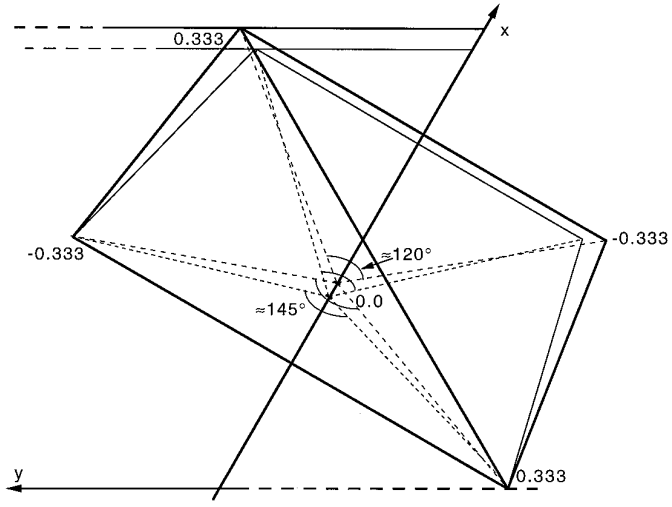

FIG. 8. Tetrahedron deformation evolution between 0.0001 and 8.51 GPa for $AlPO_4$ from (41) (The same scale has been used).

As can be seen in Fig. 11, the compressibility of M–X distances in terms of pressure is linearly related to the M–O–X angle. However, this compressibility varies in a different fashion with the cell volume. As shown in Table 1, all the known quartz-like materials can be grouped together in two classes: $V \approx 230$ Å^3 (SiO_2, $AlPO_4$, $GaPO_4$) and 245 Å^3 (GeO_2, $AlAsO_4$, $FePO_4$, $GaAsO_4$) and the compressibility increases with the cell volume. On the other hand, when the variation in the M–X–M angles and cell parameters is expressed in terms of pressure by a second order polynomial law (Figs. 9 and 10), the c/a ratio exhibits linear behavior (Fig. 12).

At high temperature, the stability of α-quartz is restricted by phase transitions or chemical decomposition. At room temperature, gradual pressure-induced amorphization is observed (at about 25–35 GPa (30)), followed at

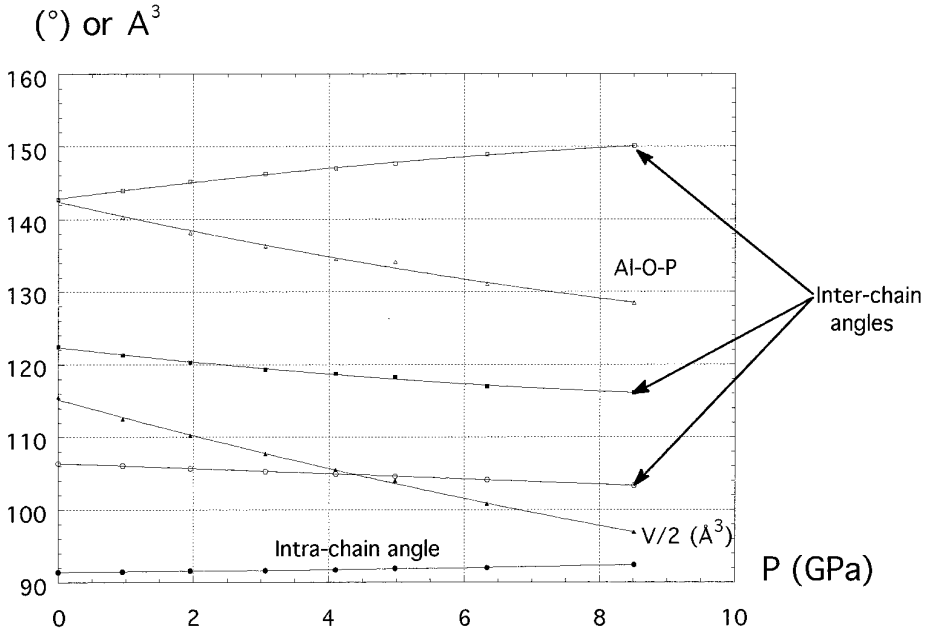

FIG. 9. Evolution of the four independent tetrahedral angles, X–M–X, of berlinite in the pressure range 0.0001–8.51 GPa compared to that of the half cell volume and the P–O–Al angle (41) (All the data have been fitted with a second order polynomial law.)

higher pressures (above 60 GPa (31)) by a transformation to a crystalline octahedrally coordinated ''rutile-like'' structure. Only a few studies have been devoted to high pressure behavior of quartz-like compounds due to experimental difficulties. Nevertheless, some interesting results can be inferred from the data in Table 3.

Higher pressure favors higher coordination and ultimately amorphization; the most surprising result is the completely reversible crystal-to-amorphous transition for $AlPO_4$ (27, 28). These crystal structure modifications seem to be linked to the crystal structure compressibility, especially along the c axis ($\Delta c/c$) (Fig. 10). A weaker $\Delta c/c$

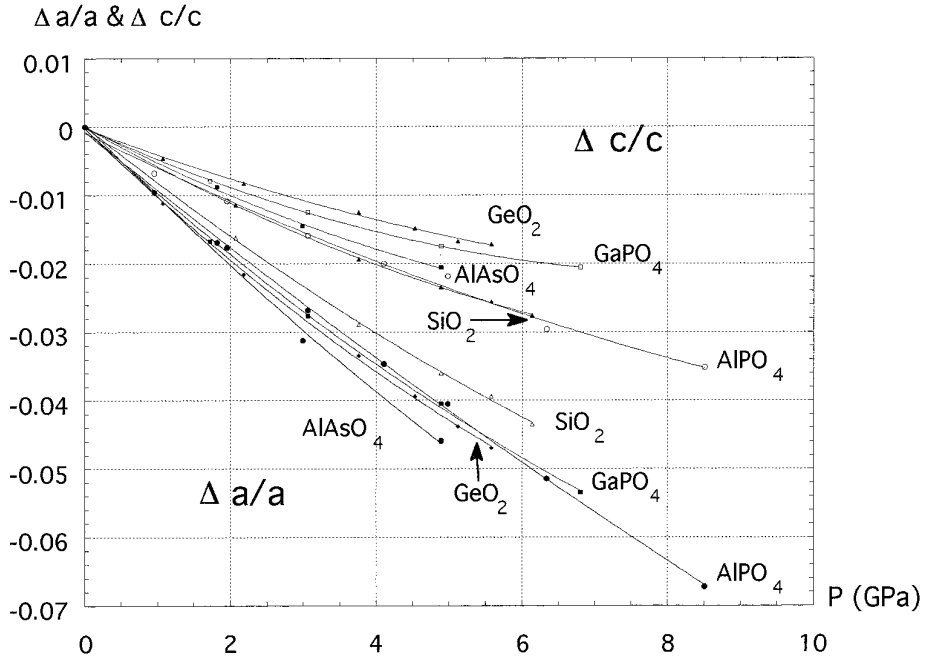

FIG. 10. $\Delta a/a$ and $\Delta c/c$ evolutions of quartz and quartz-like materials versus the pressure.

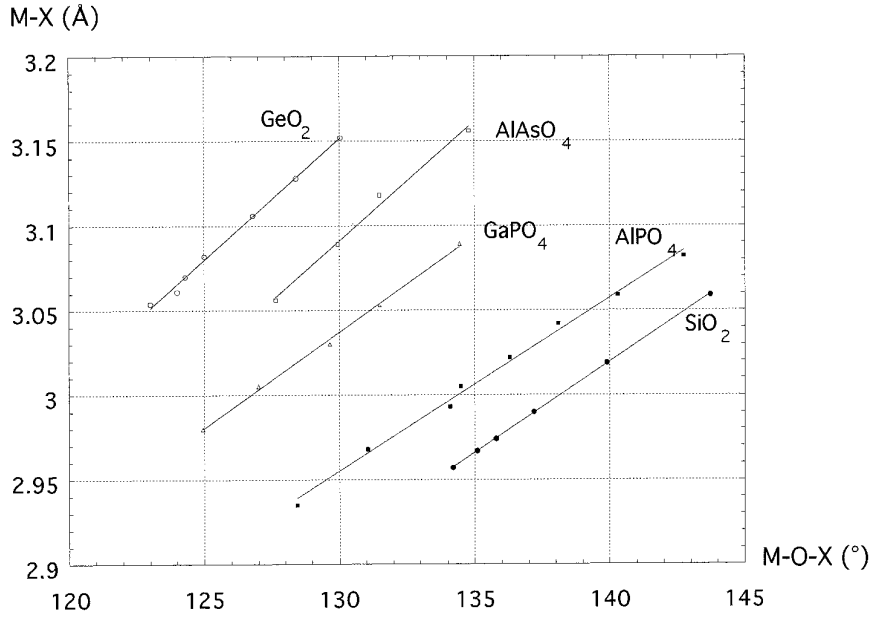

FIG. 11. Evolution of M–X length versus M–O–X angles when the pressure changes. For each material, when pressure increases the M–X distances and the M–O–X angle decreases.

sensitivity (GeO_2 and $GaPO_4$) indicates a near elasticity limit of the α-quartz crystal structure (6 and 10 GPa, respectively), whereas a higher sensitivity suggests a larger stability range to this packing (to 15 and 20 GPa for $AlPO_4$ and SiO_2, respectively).

If the temperature and pressure effects are combined, new kinds of transitions are observed: a rutile packing (SiO_2 (30), $AlAsO_4$ (45), and $GaAsO_4$ (46)) with cations in octahedral coordination, or a $CrVO_4$ packing ($AlPO_4$ (47)) with cations in both tetrahedral and octahedral coordination.

In summary, pressure and temperature effects vary in

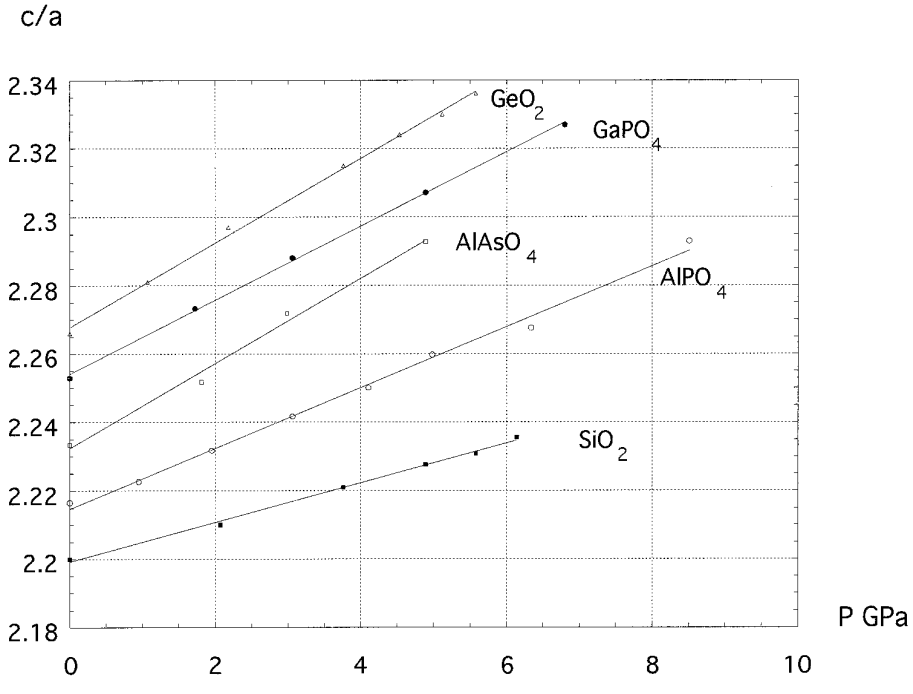

FIG. 12. Linear evolutions of the c/a ratio for quartz and quartz-like materials versus pressure. The structural distortions increase with pressure. The c/a ratio moves away the ideal value of 1.0981 for quartz and $2\times$ 1.0981 for quartz-like materials (21).

TABLE 3
Structural Behavior of α-Quartz Materials in Terms of Pressure

Material	Pressure of phase transition (GPa)	Phase transition	Reference
GeO_2	≈7–9	Partly and irreversible amorphous phase with 6 coordination for Ge atom	(25)
$GaAsO_4$	≈10	Partly reversible crystal transition with 6 coordination for Ga atom	(26)
$GaPO_4$	≈10–11	Crystal transition with 4 coordination for Ga atom	(26)
$AlPO_4$	≈15	Reversible amorphous phase	(27, 28)
SiO_2	≈25–35	Partly and irreversible amorphous phase	(30)
	>60	6 coordination for Si atom	(31)

opposite fashion with respect to bond angles (M–O–X, M–X–M, or X–M–X) and cell parameters, and the reversible distortions due to pressure effects are observed over a wider range than are temperature effects.

After this comparative survey of quartz structures in terms of pressure and temperature, the relationships between structure and physical properties are discussed. As already emphasized (15), structural parameters, such as the tilt angle or the M–O–X angle, can be closely related to the α–β transition and its existence. In this way, we have tried to correlate structural distortions and physical properties.

IV. RELATIONS BETWEEN STRUCTURES AND PHYSICAL PROPERTIES

The existence of the α–β transition can be predicted by the value of the tilt angle, δ, which is 0° in β-quartz (Fig. 1). Thus, when this angle increases, more energy is needed for the displacive transition as well as for other structural changes, such as reconstructive phase transitions or chemical decomposition, which can take place before the α–β transition. For example, Engel and Krempl (48) have predicted a theoretical value of 1929 K for the α–β $GaPO_4$ transition when the α-quartz–cristobalite transition takes place at 1206 K.

In the same way, we have attempted to reveal simple relations between structural parameters and physical properties. As a starting point, we have compared some piezoelectric and dielectric properties of the three best known materials: SiO_2, $AlPO_4$, and $GaPO_4$. Thus, in Table 4 and Fig. 13 the characteristics of the temperature compensated AT cut (coupling coefficient, k, and its angle) and the dielectric anisotropy $|\Delta\varepsilon|$ are reported. It appears clearly that dielectric and piezoelectric parameters are closely and linearly related to the structural distortions expressed by the M–O–X angle. A linear relation can also be observed when this angle is plotted against another expression of the crystal structure distortion, the c/a ratio (Fig. 2). Similarly, we can correlate the M–O–X angle to other basic physical properties, such as density (Fig. 14).

Unlike cell volumes, which can be grouped together in two classes (Table 1), the calculated densities of all the well-known quartz-like materials are linearly related to the structural distortions expressed by the bridge angle M–O–X. For the doubtful MXO_4 phases, of which structures are not still known, their density values deviate from the straight line, and we can assume that their synthesis would be impossible under the same conditions as well-known MXO_4 compounds (2–4, 9).

Thus, the AT cut characteristics of quartz, berlinite, and $GaPO_4$ being linearly related, values for all the quartz-like materials whose properties still are not known can be extrapolated, if the crystal structures have been refined (Fig. 15 and Table 5). The linear variation is confirmed by the extrapolation toward large θ angles where the coupling

TABLE 4
Comparison of Some Structural Characteristics and Experimental Properties of Quartz, Berlinite, and $GaPO_4$ Materials

Material	AT temperature compensated cut angle (°)	k (%)	Dielectric anisotropy $\lvert\Delta\varepsilon\rvert = [\varepsilon_{11}^T - \varepsilon_{33}^T]$	M–O–X (°)	c/a
Quartz	−35.25	8.5	0.12	143.7	(×2)2.20
Berlinite	−33.02	11.0	0.2	142.4	2.22
$GaPO_4$	≈−15	≈18	0.46	134.6	2.25

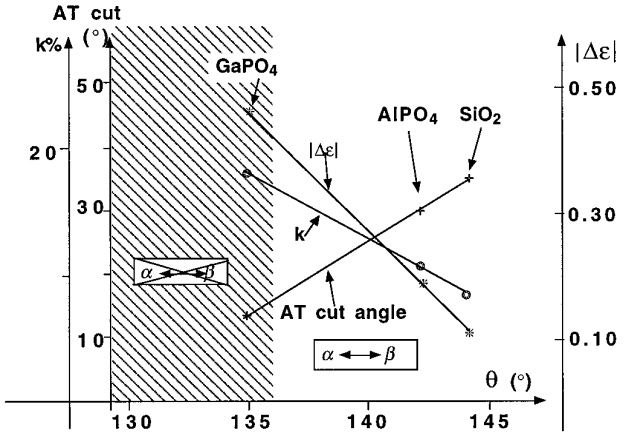

FIG. 13. Evolution of some physical characteristics of quartz, berlinite, and $GaPO_4$ crystals in terms of M–O–X bridge angle, θ. Hatched region, no α–β transition, k (%) = coupling coefficient, and $|\Delta\varepsilon|$ = dielectric anisotropy.

coefficient converges to zero, as occurs when the Si–O–Si angle equals 153° in β-quartz, a nonpiezoelectric material (10). From this extrapolation, $GaAsO_4$ and GeO_2 would appear to be the most promising materials (highest coupling coefficient for the AT cut, $k \approx 25\%$). As previously noted, a linear relation can be extrapolated in terms of the c/a ratio (Fig. 16), leading to the same coupling coefficient value for $GaAsO_4$, which reinforces the assumption.

As a final step, it would be interesting to deepen the relations between structural packing and physical behavior, in particular the piezoelectric properties. Indeed, crystal elastic moduli describe the structural deformation that takes place when a given stress is applied to a crystal. From a previous quartz study (40), one of the off-diagonal elastic moduli, c_{13}, describes the stress induced in the c direction due to a strain parallel to an a axis; the other, c_{12}, describes the similar coupling between a_1 ($a_1 = x$ axis and $a_2 = y$ axis) and the direction perpendicular to a_1 and c. When a coil spring is shortened parallel to its axis, very little stress is induced in a direction perpendicular to the axis. Analogously, compression along the c axis can be easily accomodated by the quartz structure, which is built up from tetrahedral chains that spiral around the threefold screw axis parallel to c. When a length change occurs due to compression along the c axis, the small value of c_{13} suggests that there is a small concomitant change in a. In addition, if a length change occcurs parallel to a_1, a small change in the direction perpendicular to a_1 and c results (c_{12}).

If we consider the anisotropy of all the quartz structure compressibilities expressed in terms of pressure, $(\Delta c/c)/(\Delta a/a)$, no generalized conclusions may be drawn, due to the uncertainty of $\Delta a/a$ and $\Delta c/c$ values (Fig. 17). Nevertheless, a qualitative comparison unambiguously reveals a regular decrease of the $(\Delta c/c)/(\Delta a/a)$ anisotropy ratio from the quartz to GeO_2. In other words, a given stress (or pressure) along the c axis should lead to a stronger concomitant change in the length of a from quartz to GeO_2, as c_{13} should increase. A linear evolution is confirmed by the constants of the three known crystals (Fig. 18) and gives an assumed value of $c_{13} \approx 31 \times 10^9\ \mathrm{N \cdot m^{-2}}$ for $GaAsO_4$. For

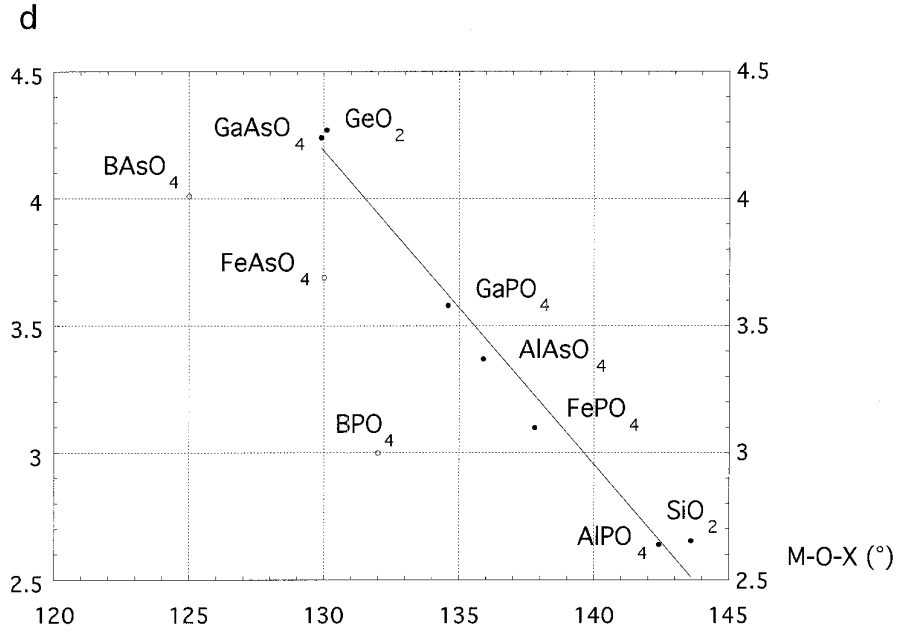

FIG. 14. Density evolution of quartz and quartz-like materials in terms of M–O–X bridge angle.

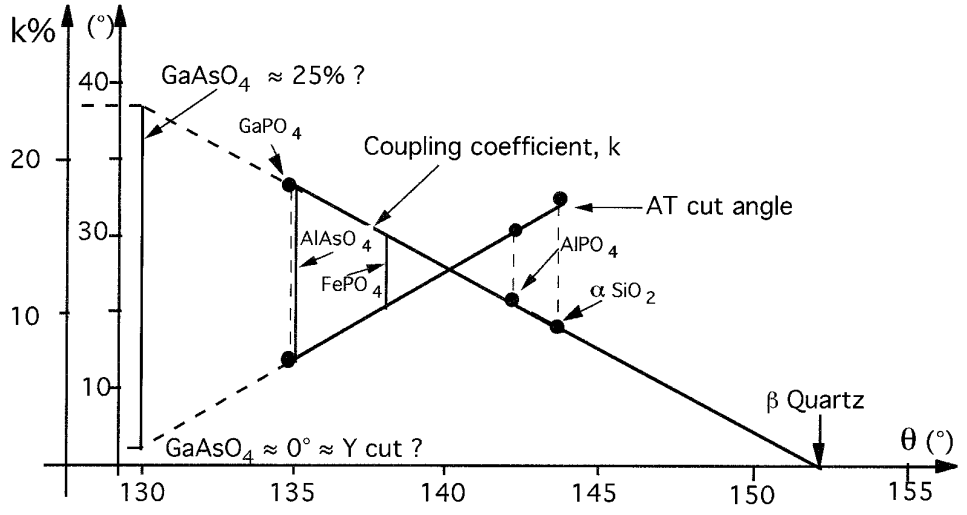

FIG. 15. Extrapolation of possible piezoelectric properties to other quartz-like materials.

the same reason, this increase of anisotropy from quartz to GeO_2 should lead to a similar evolution for c_{12}, as is also confirmed by the known constants, leading to an assumed value of $c_{12} \approx 30 \times 10^9$ N · m^{-2} for $GaAsO_4$.

The lengthening and the necking of a rod under tensile stress is described by Poisson's ratio. This coefficient, also described as the relative variations ratio occurring in the XY plan, compared to those related to the optic axis c, $(\Delta a/a)/(\Delta c/c)$, can be written in terms of K, the bulk modulus, and μ, the shear modulus: $\sigma = (3K - 2\mu)/2(3K + \mu)$. The Voigt bound of K can be expressed as $1/9[a + 2b]$, where, for the case of quartz, $a = 2c_{11} + c_{33}$ and $b = 2c_{13} + c_{12}$ (c_{ij}'s are single-crystal elastic moduli); μ can be written as $1/15[a - b + 3c]$, where a and b are as above, and $c = 2c_{44} + c_{66}$. Therefore, $\sigma = [a + 4b - 2c]/[4a + 6b + 2c]$. The value of σ for most minerals is $\sigma \approx 0.25$, which implies that the sum of the pure-shear elastic moduli (c) is approximately equal to the sum of the off-diagonal shear moduli (b). For quartz, the low σ value of 0.056 is associated with a b/c ratio of 0.2 instead of 1.0 (49), due to easily expanding and contracting spirals of tetrahedra, which behave like coiled springs (40). When quartz is compared to other known isotypes, a linear increase of Poisson's ratio is observed from quartz to berlinite and $GaPO_4$. This linearity suggests that $GaAsO_4$ has a higher value of Poisson's ratio ($\sigma \approx 0.28$), with a b/c ratio close to 1. Thus, in contrast to quartz, and in accordance with the increase of packing anisotropy $(\Delta c/c)/(\Delta a/a)$, we can assume a less easily expanding and contracting tetrahedral framework for $GaAsO_4$.

This phenomenon can also be demonstrated by considering the compressibility behavior, denoted as β, which is related to the network ability to contract under an applied isotropic hydrostatic pressure (50). Considering particularly the compressibility along a direction included in a plane perpendicular to the c axis, β_{XY}, defined as the compliance sum "$S_{11} + S_{12} + S_{13}$," and the compressibility directly related to this axis, $\beta_Z = S_{33} + 2S_{13}$, it can be clearly observed that for whatever material is probed, the β_{XY}/β_Z ratio often ranks above unity. This discrepancy increases from quartz to $GaPO_4$ (Fig. 18). Thus, the $(\Delta c/c)/(\Delta a/a)$ ratio decreases, with a concomitant Poisson's ratio increase, as predicted by direct calculation.

The other point to be noticed concerns the assumption that crystals with higher Poisson's ratio have "softer" structures, for which, other conditions being equal, an increase

TABLE 5
Extrapolation of AT Cut Characteristics from Well Known Quartz and Quartz-like Materials

Material	Sio_2	$AlPO_4$	$FePO_4$	$AlAsO_4$	$GaPO_4$	GeO_2	$GaAsO_4$
AT cut angle (°)	−35.25	−33.02	≈−20	≈−15	≈−15	≈0	≈0
coupling coefficient k (%)	8.5	11.0	≈15	≈18	≈18	≈25	≈25
c/a	2.20	2.22	2.23	2.23	2.26	2.27	2.28

TABLE 6
Compared Structural Data and Physical Properties of Quartz and Three Other Quartz-like Materials

Material parameters	SiO_2, α-quartz	$AlPO_4$, berlinite	$GaPO_4$	*$GaAsO_4$*
a, c (Å)	4.9121, 5.4044	4.937, 10.926	4.899, 11.034	4.993, 11.366
c/a	1.10 (×2 = 2.20)	2.22	2.25	2.28
V(Å^3)	113 (×2 = 226)	231	229	245
d	2.655	2.640	3.570	4.155
M–O–X	143.7	142.4	134.6	129.9
δ(°)	16.3	17.6	23.3	26.2
AT cut angle (°)	−35.25	−33.02	≈−15	*≈0*
AT cut coupling coefficient, k	0.085	0.11	0.18	*≈0.25*
Poisson's ratio	0.056	0.105	0.208	*≈0.28*
β_{XY}/β_Z	1.35	1.62	1.94	*≈2.23*
$d_{11}(10^{-12}\mathrm{C}\cdot\mathrm{N}^{-1})$	2.31*	3.30*	4.5*	
$d_{14}(10^{-12}\mathrm{C}\cdot\mathrm{N}^{-1})$	0.727*	1.62*	1.9*	
$S_{11}(10^{-12}\mathrm{N}\cdot\mathrm{m}^{-2})$	12.78*	16.4*	17.93*	
$S_{12}(10^{-12}\mathrm{N}\cdot\mathrm{m}^{-2})$	−1.77*	−3.2*	−4.82*	
$S_{13}(10^{-12}\mathrm{N}\cdot\mathrm{m}^{-2})$	−1.25*	−2*	−3.19*	
$S_{14}(10^{-12}\mathrm{N}\cdot\mathrm{m}^{-2})$	−4.53*	−5.9*	−2.36*	
$S_{33}(10^{-12}\mathrm{N}\cdot\mathrm{m}^{-2})$	9.74*	11.9*	11.35*	
$S_{44}(10^{-12}\mathrm{N}\cdot\mathrm{m}^{-2})$	20.00*	26.8*	27.04*	
$S_{66}(10^{-12}\mathrm{N}\cdot\mathrm{m}^{-2})$	29.10*	39.2*	45.50*	
$c_{11}(10^{9}\mathrm{N}\cdot\mathrm{m}^{-2})$	86.79*	64.88*	66.6*	
$c_{12}(10^{9}\mathrm{N}\cdot\mathrm{m}^{-2})$	6.79*	8.98*	21.8*	*≈30*
$c_{13}(10^{9}\mathrm{N}\cdot\mathrm{m}^{-2})$	12.01*	14.6*	24.9*	*≈31*
$c_{14}(10^{9}\mathrm{N}\cdot\mathrm{m}^{-2})$	18.12*	−12.17*	3.9*	
$c_{33}(10^{9}\mathrm{N}\cdot\mathrm{m}^{-2})$	105.79*	87.14*	102.1*	
$c_{44}(10^{9}\mathrm{N}\cdot\mathrm{m}^{-2})$	58.21*	43.12*	37.7*	
$c_{66}(10^{9}\mathrm{N}\cdot\mathrm{m}^{-2})$	40.00*	27.95*	22.4*	

Note. Italic denotes extrapolated values.
* Convention IEEE 1978 Left Crystal.

in the piezoelectric properties is observed (51). The coupling coefficient behavior, as well as the d_{ik}/S_{kk} ratios (Fig. 18), are in total agreement with this point of view.

Other relations between structures and physical properties can be extrapolated in terms of packing distortions (or M–O–X angles). So, it has been predicted that better thermal stability (closely related to the resonance frequency temperature coefficients), and a slower acoustic wave velocity (52) result when the M–O–X distortion increases from quartz to berlinite, $GaPO_4$, and $GaAsO_4$.

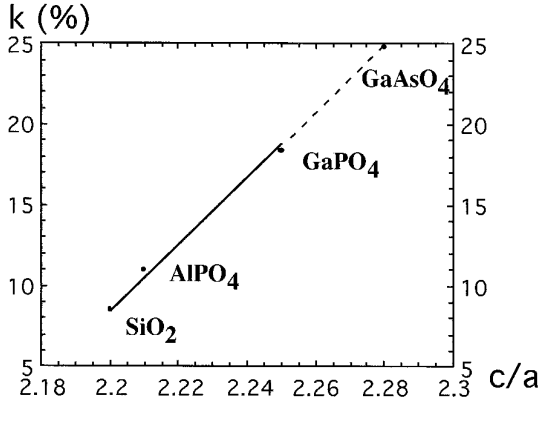

FIG. 16. Extrapolated coupling coefficient for $GaAsO_4$ in terms of the c/a ratio.

V. CONCLUSION

In Table 6, we have summarized the most important characteristics of quartz and three quartz-like materials. In this paper, we tried to correlate physical properties in terms of some simple structural considerations, such as the c/a ratio, the bridge angle M–O–X, and the nonbonded distance M–X.

The increasing value of the c/a ratio and of the intratetrahedral distortions with the reduction of the M–O–X angle from quartz to $GaAsO_4$ reflect increases in the distortion of the whole crystal structure. A schematic description of these structural changes has been proposed in terms of only the heavy cations, M and X, and all the intertetrahedral angles, M–X–M or X–M–X, are linearly related to the M–O–X angle.

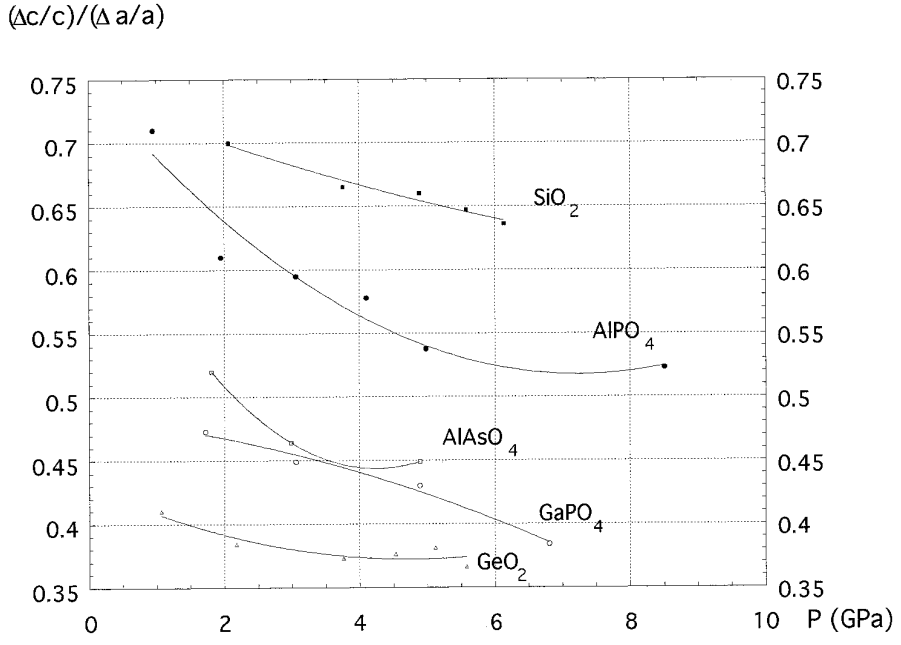

FIG. 17. Variation of the anisotropy, $(\Delta c/c)/(\Delta a/a)$, of quartz and quartz-like materials against the pressure.

From temperature and pressure effects on the structural packing, it can be observed that the compressibility along the helical chain is less pronounced than the compressibility associated with the packing of chains. Temperature and pressure have opposite effects on angles (M–O–X, M–X–M, or X–M–X) and cell parameters. Reversible distortions due to pressure effects occur over a wider range than distortions that are induced by temperature.

On the other hand, close relations exist between the crystal structure distortions, expressed in terms of the M–O–X angle value, and different physical properties. For instance, piezoelectric characteristics of the AT cut and

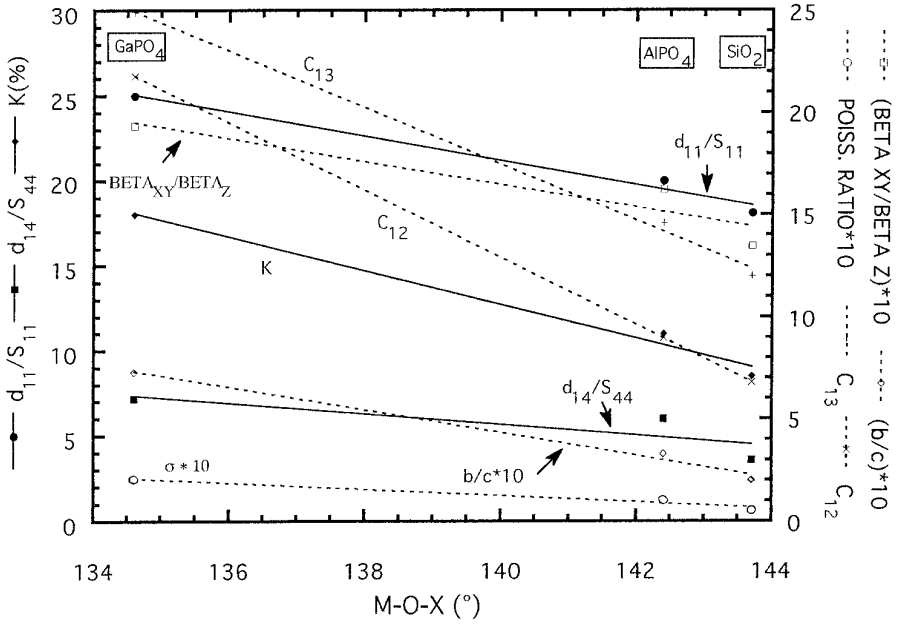

FIG. 18. Evolution versus the M–O–X bridging angle of (in the left scale) the coupling coefficient k (%), the d_{ik}/S_{kk} (10^{-2} C · m^{-2}) ratio; and (in the right scale) the elastic moduli c_{12} and c_{13} (10^9 N · m^{-2}), β_{XY}/β_Z (×10), b/c ratio (×10), and Poisson's ratio σ (×10).

dielectric constant anisotropy of three known materials (SiO_2, $AlPO_4$, and $GaPO_4$) have been linearly related successfully to their M–O–X angle value. Conversely, knowledge of the M–O–X value allows prediction of physical properties for quartz-like crystals that have not been synthesized. Consequently, using only M–O–X angles, one can describe the structural strains, the α–β transition existence, and some physical properties, such as density, piezoelectric characteristics, and elastic constants.

Based on this reasoning, $GaAsO_4$ and GeO_2 appear to be the most promising materials for piezoelectric applications. Unfortunately, the concomitant increase in structural distortions from quartz to $GaAsO_4$ and GeO_2 make their crystal growth very difficult. From our crystal growth experience, $GaPO_4$ seems to be the best compromise for industrial development, having high AT cut coupling coefficient and large temperature range stability with few drastic packing distortions.

ACKNOWLEDGMENTS

The authors acknowledge the DRET and the CNRS for their financial support.

REFERENCES

1. A. Goiffon, J. C. Jumas, M. Maurin, and E. Philippot, *J. Solid State Chem.* **61,** 384 (1986).
2. J. C. Jumas, A. Goiffon, A. Zarka, B. Capelle, J. C. Doukhan, J. Schwartzel, J. Detaint, and E. Philippot, *J. Cryst. Growth* **80,** 133 (1987).
3. A. Goiffon, A. El Bouchikhi, J. C. Jumas, C. Avinens, M. Maurin, and E. Philippot, *Eur. J. Solid State Inorg. Chem.* **25**(2), 201 (1988).
4. E. Philippot, A. Goiffon, M. Maurin, J. Detaint, J. Schwartzel, Y. Toudic, B. Capelle, and A. Zarka, *J. Cryst. Growth* **104,** 713 (1990).
5. J. Detaint, H. Carru, J. Schwartzel, C. Joly, B. Capelle, A. Zarka, and E. Philippot, *Proc. 45th Ann. Freq. Control Symp.* 166 (1991).
6. J. Detaint, J. Schwartzel, C. Joly, B. Capelle, A. Zarka, Y. Zheng, Y. Toudic, and E. Philippot, *Proc. 6th Eur. Freq. Time Forum* 223 (1992).
7. J. Detaint, J. Schwartzel, C. Joly, A. Zarka, B. Capelle, Y. Zheng, and E. Philippot, *Proc. 6th Eur. Freq. Time Forum* 383 (1992).
8. D. Cachau, J. Bennazha, A. Goiffon, A. Ibanez, and E. Philippot, *Eur. J. Solid State Inorg. Chem.* **29,** 1295 (1992).
9. E. Philippot, A. Ibanez, A. Goiffon, M. Cochez, A. Zarka, B. Capelle, J. Schwartzel, and J. Detaint, *J. Cryst. Growth* **130,** 195 (1993).
10. G. Dolino, J. P. Bacheimer, F. Gervais, and A. F. Wright, *Bull. Minér.* **106,** 267 (1983).
11. T. Rey, *Z. Kristallogr.* **123,** 263 (1966).
12. E. C. Shafer and R. Roy, *J. Am. Ceram. Soc.* **39,** 330 (1956).
13. E. C. Shafer, M. W. Shafer, and R. Roy, *Z. Kristallogr.* **108,** 263 (1956).
14. K. Kosten and H. Arnold, *Z. Kristallogr.* **152,** 119 (1980).
15. E. Philippot, A. Goiffon, A. Ibanez, and M. Pintard, *J. Solid State Chem.* **110,** 356 (1994).
16. C. Glidewell, *Inorg. Chim. Acta* **12,** 219 (1975).
17. M. O'Keefe and B. G. Hyde, *Trans. Am. Cryst. Assoc.* **15,** 65 (1979).
18. M. O'Keefe and A. Navrotsky, "Structure and Bonding in Crystals." Academic Press, New York, 1981.
19. R. D. Shannon and C. T. Prewitt, *Acta Crystallogr. B* **25,** 925 (1969).
20. H. Grimm and B. Dorner, *J. Phys. Chem. Solids* **36,** 407 (1975).
21. G. S. Smith, *Acta Crystallogr.* **16,** 542 (1963).
22. R. J. Hill and G. V. Gibbs, *Acta Crystallogr. B* **35,** 25 (1979).
23. W. R. Beck, *J. Am. Ceram. Soc.* **32,** 147 (1949).
24. K. Allaf and A. Rouanet, *High Temp. High Pressures* **10,** 591 (1978).
25. J. P. Itie, A. Polian, G. Calas, J. Petiau, A. Fontaine, and H. Tolentino, *Phys. Rev. Lett.* **63,** 398 (1989).
26. J. P. Itie, T. Tinoco, A. Polian, G. Demazeau, S. Matar, and E. Philippot, *High Pressure Res.* in press.
27. M. B. Kruger and R. Jeanloz, *Science* **249,** 647 (1990).
28. A. Polian, M. Grimsditch, and E. Philippot, *Phys. Rev. Lett.* **71,** 3143 (1993).
29. R. M. Hazen, L. W. Finger, R. J. Hemley, and H. K. Mao, *Solid State Commun.* **72,** 507 (1989).
30. R. J. Hemley, A. P. Jephcoat, H. K. Mao, L. C. Ming, and M. H. Manghnani, *Nature* **334,** 52 (1988).
31. N. Binggeli and J. R. Chelikowsky, *Nature* **353,** 344 (1991).
32. K. Kihara, *Eur. J. Miner.* **2,** 63 (1990).
33. G. A. Lager, J. D. Jorgensen, and F. J. Rotella, *J. Appl. Phys.* **53,** 6751 (1982).
34. R. J. Ackermann and C. A. Sorrell, *J. Appl. Crystallogr.* **7,** 461 (1974).
35. Y. Le Page, L. D. Calvert, and E. J. Gabe, *J. Phys. Chem. Solids* **41,** 721 (1980).
36. O. Baumgartner, A. Preisinger, P. W. Krempl, and H. Mang, *Z. Kristallogr.* **168,** 83 (1984).
37. O. Baumgartner, M. Behmer, and A. Preisinger, *Z. Kristallogr.* **187,** 125 (1989).
38. J. D. Jorgensen, *J. Appl. Phys.* **49,** 5473 (1978).
39. H. D'Amour, W. Denner, and H. Schulz, *Acta Crystallogr. B* **35,** 550 (1979).
40. L. Lieven, C. T. Prewitt, and D. J. Weidner, *Am. Miner.* **65,** 920 (1980).
41. H. Sowa, J. Macavei, and H. Schulz, *Z. Kristallogr.* **192,** 119 (1990).
42. H. Sowa, *Z. Kristallogr.* **194,** 291 (1991).
43. H. Sowa, *Z. Kristallogr.* **209,** 954 (1994).
44. J. Glinnemann, H. E. King, H. Schulz, T. Hahn, S. J. La Placa, and F. Dacol, *Z. Kristallogr.* **198,** 177 (1992).
45. A. R. Young, C. B. Sclar, and C. M. Schwarz, *Z. Kristallogr.* **118,** 223 (1963).
46. S. Matar, M. Lelogeais, D. Michau, V. Ferris, and G. Demazeau, *High Pressure Res.* **7,** 117 (1991).
47. K. F. Seifert, *Fortschr. Mineral.* **45,** 214 (1968).
48. G. F. Engel and P. W. Krempl, *Ferroelectrics* **54,** 9 (1984).
49. H. J. McSkimin, P. Andreatch, Jr., and R. N. Thurston, *J. Appl. Phys.* **38,** 347 (1965).
50. H. A. A. Sidek, G. A. Saunders, Wang Hong, Xu Bin, and Han Jianru, *Phys. Rev. B* **36,** 7612 (1987).
51. I. M. Sil'Vestrova, Yu. V. Pisarevskii, O. V. Zvereva, and A. A. Shternberg, *Sov. Phys. Crystallogr.* **32,** 467 (1987).
52. J. Detaint, J. Schwartzel, A. Zarka, B. Capelle, E. Philippot, and J. P. Denis, *Proc. 48th IEEE Inter. Freq. Control Symp.* in press.